

General Disclaimer

One or more of the Following Statements may affect this Document

- This document has been reproduced from the best copy furnished by the organizational source. It is being released in the interest of making available as much information as possible.
- This document may contain data, which exceeds the sheet parameters. It was furnished in this condition by the organizational source and is the best copy available.
- This document may contain tone-on-tone or color graphs, charts and/or pictures, which have been reproduced in black and white.
- This document is paginated as submitted by the original source.
- Portions of this document are not fully legible due to the historical nature of some of the material. However, it is the best reproduction available from the original submission.

SOME ASPECTS OF
FATIGUE CRACK PROPAGATION

by

Richard Roberts and John J. Kibler

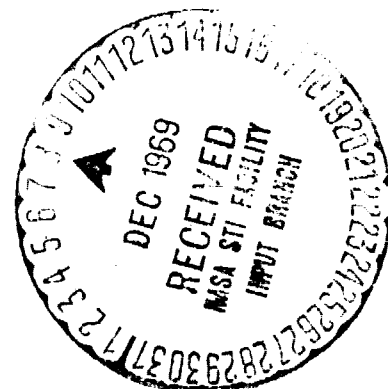
N70-12325

FACILITY FORM 602

(ACCESSION NUMBER)	(THRU)
32	1
(PAGES)	(CODE)
CR-66829	32
(NASA CR OR TMX OR AD NUMBER)	(CATEGORY)

Prepared under Grant No. NGR-39-007-011
and under NSF Grant GK-1225 by
LEHIGH UNIVERSITY
Bethlehem, Pa.
for
NATIONAL AERONAUTICS AND SPACE ADMINISTRATION

July 1969



SOME ASPECTS OF
FATIGUE CRACK PROPAGATION

by Richard Roberts and John J. Kibler

Lehigh University, Bethlehem, Pa.

SUMMARY

The models of fatigue crack propagation proposed by Forman et al and Roberts and Erdogan were studied in this paper. By applying these models to existing data in the literature for thin 2024-T3 and 7075-T6 aluminum plates subjected to fluctuating tensile loads, it was found that both models gave comparable results when one considered just a gross correlation of the experimental data. By modifying Forman's model to incorporate the ideas of Roberts and Erdogan, a model was produced which appeared to be a more rational basis for studying the problem of fatigue crack propagation in thin plates and shells subjected to tensile loads, bending loads, or a combination of both. This fact was demonstrated for the case of thin plates subjected to fluctuating bending loads and for the case of thin cylindrical shells subjected to fluctuating internal pressure.

This paper also presents the large quantity of data relating the rate of fatigue crack propagation in thin plates subjected to fluctuating bending loads collected at Lehigh University.

INTRODUCTION

Recent work (refs. 1, 2, and 3) has clearly shown that the rate of fatigue crack propagation in thin sheets subjected to either fluctuating tensile loads or fluctuating bending loads is related to the stress-intensity factor.

It is the purpose of this paper to evaluate the fatigue crack propagation models of Forman et al (ref. 2) and Roberts and Erdogan (ref. 3). This evaluation will be limited to two aluminum alloys, 2024-T3 and 7075-T6. The primary source of data for fatigue crack propagation due to plane extension used in this evaluation will be the work of Donaldson and Anderson (ref. 4) and the work of Schijve and his co-workers (ref. 5). The data relating the effect of bending loads on fatigue crack propagation comes from the extensive work performed at Lehigh University during the past few years.

Since the large quantity of data gathered at Lehigh University relating the rate of fatigue crack propagation to fluctuating bending loads is not readily available in the literature, it is the secondary purpose of this paper to present these data in a convenient form whereby other researchers may make use of these data. To date, none of

the raw data and only a partial analysis of some of the data appears in the literature (refs. 3 and 6).

FATIGUE CRACK PROPAGATION MODELS

Many functional forms have been proposed to represent the relationship between the rate of fatigue crack propagation and various physical parameters.

Paris and Erdogan (ref. 1) proposed the following relationship between the rate of fatigue crack propagation and the stress-intensity factor amplitude, ΔK :

$$\frac{da}{dN} = A(\Delta K)^m \quad (1)$$

where a is the half crack length for a center-cracked specimen, N is the number of load cycles, ΔK is the stress-intensity factor amplitude defined herein as $\Delta K = (K_{\max} - K_{\min})/2$, A is a constant which must be determined for each material, mean load, etc., and m is a numerical exponent. Paris and Erdogan found the general trend of the data indicated that $m \approx 4$.

Forman et al (ref. 2) argued that a correct crack growth law should include the criterion that the crack growth rate approach infinity as the maximum value of the stress-intensity factor, K_{\max} , approaches the stress-intensity

level for rapid fracture, K_C . Thus by modifying the model of Paris and Erdogan, equation 1, Forman et al proposed an equation of the form

$$\frac{da}{dN} = \frac{B(\Delta K)^n}{(1-R)K_C - 2\Delta K} \quad (2)$$

where $R = K_{min}/K_{max}$, K_C is the critical stress-intensity factor for rapid fracture, B is a material constant, and n is a numerical exponent.

In evaluating their model, Forman et al used the data found in (refs. 4, 5, and 7). For the aluminum alloys 2024-T3 and 7075-T6, they found $n \approx 3$. They also found the values of K_C which best fit the data were in reasonable agreement with published values of K_C .

Erdogan and Roberts (refs. 3 and 6) proposed that the rate of fatigue crack propagation is probably more fundamentally related to the size of the plastic zone ahead of and in the plane of the fatigue crack. This led to an equation of the form

$$\frac{da}{dN} = C(K_{max})^p (\Delta K)^q \quad (3)$$

where C is a material constant, and p and q are numerical exponents. They found for tensile and bending loads that the values of p and q in equation (3), for 2024-T3 and

7075-T6 aluminum alloys, could be approximated as
 $p = q \approx 2$.

EXPERIMENTAL RESULTS

The results of two experimental programs are reported in this paper. In the first program, 2024-T3 and 7075-T6 aluminum plates which contained a central through crack were subjected to fluctuating cylindrical bending loads. Reference (6) gives a detailed description of the testing equipment and procedures used for collecting the data. Appendix A contains the values of the crack length, number of cycles, specimen thickness, load levels, etc., for these tests.

The second program consisted of subjecting 2024-T3 bare aluminum plates containing a central through crack to a combined static tensile load and a cyclic transverse bending load. Reference (12) gives a detailed description of the testing equipment and procedures. The results obtained from the combined loading tests are given in Appendix B.

The mechanical properties of the combined loading specimens and the cylindrical bending specimens are given in Appendix C. The values listed in this appendix are the

average values for four test specimens. These mechanical properties were determined in accordance with the appropriate ASTM standard for sheet material.

DISCUSSION

The bending data given in the Appendices will not be discussed in detail in this paper. These data will be used solely as a means of comparing the models of Forman et al and Roberts and Erdogan.

The quantity β was introduced into equations (2) and (3) before making the comparison of these equations. β is defined as $\beta = K_{\text{mean}}/\Delta K$ where $K_{\text{mean}} = (K_{\text{max}} + K_{\text{min}})/2$. Thus equations (2) and (3) can be written as

$$\frac{da}{dN} = \frac{B(1 + \beta)(\Delta K)^n}{K_c - (1 + \beta)\Delta K} \quad (4)$$

and

$$\frac{da}{dN} = C(1 + \beta)^p(\Delta K)^{p+q} \quad (5)$$

To compare equations (4) and (5) the logarithm of both sides of equations (4) and (5) were taken. The resulting equations, linear in B , C , n , p , and q , were fit to the available data using a least squares fit program. The program calculated the standard error,

$S_{y,x}$, along with the values of B, C, n, p, and q. For this program

$$S_{y,x} = \sqrt{\frac{\sum_{i=1}^M \left[\ln\left(\frac{da}{dN}\right)_{i_{\text{observed}}} - \ln\left(\frac{da}{dN}\right)_{i_{\text{calculated}}} \right]^2}{M}} \quad (6)$$

where M is the number of data pairs used in the curve fit. It was decided that the standard error was the best means of comparing the two equations. The equation which consistently had the smaller standard error would be the one which best fit the data. Since the standard error is being used as the measure of comparison, figures showing how equations (4) and (5) fit the experimental data were not prepared. The reader is referred to references (2), (3), and (6) for such figures.

Unfortunately or fortunately, depending on one's point of view, both equations gave almost identical results. The standard errors associated with fitting the values of B and C to equations (4) and (5) for the values of K_c and n recommended by Forman et al and the values of p and q recommended by Roberts and Erdogan are given in Tables 1 and 2. By comparing the values of $S_{y,x}$ in these tables, it is seen that the two equations give comparable

results. It should be noted that the best fit values of B , C , n , p , and q , along with the associated standard error were calculated for equations (4) and (5). These results, although not included in this paper, indicate that the value of $n = 3$ recommended by Forman et al, and $p = q = 2$ recommended by Roberts and Erdogan were in reasonable agreement with the least squares fit of the data. The standard errors for this case again showed that the two equations give comparable results.

It is the opinion of the present authors that the assumption made by Forman et al is correct in view of the data considered to date. The reasons for this are as follows:

- 1) The equation proposed gives excellent results when predicting the effect of mean stress on fatigue crack propagation due to plane extension for the two aluminum alloys considered.
- 2) The value of K_C in the equation of Forman et al is in good agreement with values of K_C obtained from fracture tests.

It is also the opinion of the present authors that the assumptions put forward by Roberts and Erdogan are correct. One reason for this is the ability of their

model to handle the effect of mean stress on fatigue crack propagation. A second and more important reason is the ability of their model to predict the rate of fatigue crack propagation due to bending loads from data obtained in tensile tests.

By using the argument that fatigue crack propagation is more fundamentally related to plastic zone size and by observing the similarity of fracture modes between the cylindrical bending tests given in Appendix A and results from plane extension, Roberts and Erdogan argued that for the same material if the plastic zone sizes for the two types of loading are the same, the growth rates should be the same. This led to the conclusion that the rate of fatigue crack propagation due to bending loads could be predicted from data obtained from tension testing. By modifying the stress-intensity factor for bending by a factor of $1/2$ and using the value of C in equation (5) obtained from tensile data, one has

$$\frac{da}{dN} = C(1 + \beta)^2 \left(\frac{\Delta K_b}{2} \right)^4 \quad (7)$$

where ΔK_b is the amplitude of the bending stress-intensity factor. The factor $1/2$ was determined theoretically so that the plastic zone sizes for both cases would be the same. Equation (7) was considered in reference (3).

Excellent results were obtained in predicting the fatigue crack propagation rates associated with the data given in Appendix A from fatigue crack propagation rates found in the literature for tensile data.

In a recent study, Catanach (ref. 10) investigated the rate of fatigue crack propagation in thin 6063-T6 aluminum shells. In his tests he subjected the shells which contained a longitudinal through crack to fluctuating internal pressure. As a result of the shell curvature the area near the crack tip is simultaneously subjected to varying tensile and bending loads. Using the results of Roberts and Erdogan (refs. 3 and 6), it can be shown that the plastic zone size can be approximated in the Dugdale sense (ref. 11) as being proportional to the square of $K_t + K_b/2$, where K_t is the stress-intensity factor for the in-plane tensile loads and K_b is the stress-intensity factor for the bending loads. Catanach fit equation (5) to his data. He found that he got good results using a value of $\Delta K = \Delta K_t + \Delta K_b/2$ in equation (5). Unfortunately the levels of K_b compared to K_t were so small that it was impossible to tell if the quantity $K_t + K_b/2$ was the reason for the good fit.

Based on the previous thoughts concerning the models

of Forman et al and Roberts and Erdogan and the work of Catanach, an equation of the form

$$\frac{da}{dN} = D \left(\frac{K_{max}}{K_C - K_{max}} \right)^r (\Delta K)^s \quad (8)$$

was fit to the data used to compare equations (4) and (5). The best fit values of r and s were $r \approx 1$, $s \approx 3$. Thus fixing the values of r and s at 1 and 3 respectively, one arrives back at Forman's equation:

$$\frac{da}{dN} = \frac{B(1 + \beta)(\Delta K)^3}{K_C - (1 + \beta)\Delta K}$$

The hypothesis of Roberts and Erdogan about the relationship between fatigue crack propagation rates due to tension and bending was tested by writing equation (4) as

$$\frac{da}{dN} = \frac{B(1 + \beta) \left(\frac{\Delta K_b}{2} \right)^3}{K_C - (1 + \beta) \left(\frac{\Delta K_b}{2} \right)} \quad (9)$$

This equation was fit to the data found in Appendix A for the 0.05 inch thick 2024-T3 aluminum for $\beta = 0.392, 0.632$, and 1.0. The value of B found was 2.78×10^{-12} . This compares very well with the value of B given in Table 3 for the 0.04 inch material from reference (5), $C = 2.94 \times 10^{-12}$.

As a result of the above considerations, the following modification of Forman's equation is proposed:

$$\frac{da}{dN} = \frac{C(1 + \beta)(\Delta K_e)^3}{K_c - (1 + \beta)\Delta K_e} \quad (10)$$

where K_e is defined as

$$K_e = K_t \quad ; \text{ for plane extension}$$

$$K_e = K_b/2 \quad ; \text{ for bending}$$

$$K_e = K_t + K_b/2 \quad ; \text{ for combined loading}$$

and K_t and K_b are the stress-intensity factors for extension and bending, respectively. This equation incorporates the concept of Forman et al that the fatigue crack propagation rate should become infinite as K_{max} approaches K_c . It also incorporates the concept of Roberts and Erdogan that for similar fracture modes but different types of loading, the rate of fatigue crack propagation should be the same if the plastic zone sizes are the same.

With regard to the transverse bending tests, a suitable model for estimating the plastic zone size due to the combined axial and transverse load has not been developed. When this is done a method for determining K_e in equation (10) will be available.

SUMMARY OF RESULTS

1. The equations proposed by Forman et al and Roberts and Erdogan both handle the effect of mean stress on fatigue crack propagation equally well.
2. The following equation, a modification of Forman's equation, is proposed in place of the equations of Forman et al and Roberts and Erdogan:

$$\frac{da}{dN} = \frac{B(1 + \beta)(\Delta K_e)^3}{K_c - (1 + \beta)\Delta K_e}$$

where K_e is defined as

$$K_e = K_t \quad ; \text{ for plane extension}$$

$$K_e = K_b/2 \quad ; \text{ for bending}$$

$$K_e = K_t + K_b/2 \quad ; \text{ for combined loading}$$

and K_t and K_b are the stress-intensity factors for extension and bending, respectively.

In closing, the authors would like to point out that the equation proposed was evaluated for only two aluminum alloys. Other materials might not show agreement with the equation. The hypothesis that $K_e = K_t + K_b/2$

must be viewed with caution until it can be compared to more substantial data than found in reference (10). In general a large number of questions are not answered by equation (10) and should be the object of future studies.

REFERENCES

1. P. C. Paris and F. Erdogan, "A Critical Analysis of Crack Propagation Laws," *Journal of Basic Engineering*, Trans. ASME, Series D, vol. 85, 1963, pp. 528-534.
2. R. G. Forman, V. E. Kearney, and R. M. Engle, "Numerical Analysis of Crack Propagation in Cyclic-Loaded Structures," *Journal of Basic Engineering*, Trans. ASME, Series D, vol. 89, 1967, pp. 459-463.
3. R. Roberts and F. Erdogan, "The Effect of Mean Stress on Fatigue Crack Propagation in Plates Under Extension and Bending," *Journal of Basic Engineering*, Trans. ASME, Series D, vol. 89, 1967, pp. 885-892.
4. D. R. Donaldson and W. E. Anderson, "Crack Propagation Behavior of Some Airframe Materials," *Proceeding of the Crack Propagation Symposium*, Cranfield, England, 1961.
5. *Reports and Transactions*, National Aero- and Astronautical Research Institute, Amsterdam, XXXI, 1965.
6. F. Erdogan and R. Roberts, "A Comparative Study of Crack Propagation in Plates Under Extension and Bending," *Proceeding, International Conference on Fracture*, Sendai, Japan, 1965.

7. W. Illg and A. J. McEvily, "The Rate of Fatigue Crack Propagation for Two Aluminum Alloys Under Completely Reversed Loading," NASATND-52, Oct. 1959.
8. J. R. Rice, "Mechanics of Crack Tip Deformation and Extension by Fatigue," Fatigue Crack Propagation, ASTM STU 415, Am. Soc. Testing Mats., 1967, pp. 247-309.
9. C. M. Hudson and J. T. Scardina, "Effect of Stress Ratio on Fatigue Crack Growth in 7075-T6 Aluminum Alloy Sheet," presented at the National Symposium on Fracture Mechanics, Bethlehem, Pa., 1967.
10. W. M. Catanach, Jr., "A Study of Fatigue Crack Propagation in Thin Cylindrical Shells Containing a Meridional Crack," A Ph.D. Thesis, Lehigh University, 1967.
11. D. S. Dugdale, "Yielding of Steel Sheets Containing Slits," Jour. Mech. Phys. Solids, vol. 8, 1960, pp. 100-104.
12. W. J. Valentine, "On the Rate of Crack Extension Due to Transverse Shear Fatigue Loading," M.S. Thesis, Lehigh University, 1965.

TABLE 1

Material Constant and Standard Error for
the Equation of Roberts and Erdogan

$$\frac{da}{dN} = C(1 + \beta)^2 \Delta K^4$$

Material	Reference	Thickness	C x 10 ⁻²¹	S _{y,x}
2024-T3	5	0.080	15.89	0.6167
		0.024	7.48	0.7444
		0.040	7.49	0.4112
		0.079	6.52	0.5680
		0.118	10.26	0.3144
		0.157	12.51	0.3802
	4	0.020	6.92	0.6153
		0.032	8.12	0.3266
		0.040	5.73	0.4017
		0.063	7.49	0.4807
		0.081	4.26	0.4892
		0.102	10.19	0.6469
	7	0.081	5.01	0.5503
7075-T6	5	0.080	82.27	0.4189
	4	0.064	22.20	0.4150
		0.090	23.81	0.1717
		0.102	24.41	0.5888
	7	0.081	5.31	0.5527
	9	0.090	11.23	0.5818

TABLE 2

Material Constant and Standard Error for
the Equation of Forman et al.

$$\frac{da}{dN} = \frac{B(1 + \beta)\Delta K^3}{K_C - (1 + \beta)\Delta K}$$

2024-T3 ; $K_C = 47,000$
7075-T6 ; $K_C = 38,500$

Material	Reference	Thickness	$C \times 10^{-12}$	$S_{y,x}$
2024-T3	5	0.080	2.69	0.3670
		0.024	2.89	0.7314
		0.040	2.94	0.4355
		0.079	2.60	0.4546
		0.118	4.09	0.2809
		0.157	5.02	0.4006
	4	0.020	2.55	0.5310
		0.032	3.16	0.4223
		0.040	2.20	0.2652
		0.063	2.08	0.2730
		0.081	1.07	0.2517
		0.102	3.30	0.5109
	7	0.081	1.53	0.5601
7075-T6	5	0.080	10.07	0.3489
	4	0.064	6.43	0.3327
		0.090	7.06	0.2835
		0.102	5.28	0.3278
	7	0.081	1.22	0.3257
	9	0.090	3.02	0.5466

APPENDIX A

Crack Growth Data For Cylindrical Bending

Plate Number	Material	Thickness (in.)	σ_a (PSI)	$\beta = (\sigma_m/\sigma_a)$
1	2024-T3 Clad	0.050	12,500	0
2	2024-T3 Clad	0.050	16,640	0
3	2024-T3 Clad	0.050	18,850	0
4	2024-T3 Clad	0.050	18,850	0
5	2024-T3 Clad	0.050	18,850	0
6	2024-T3 Bare	0.050	12,175	0.39
7	2024-T3 Bare	0.050	12,175	0.39
8	2024-T3 Bare	0.050	12,435	0.62
9	2024-T3 Bare	0.050	12,435	0.62
10	2024-T3 Bare	0.050	8,320	1
11	2024-T3 Bare	0.050	8,320	1
12	2024-T3 Bare	0.080	21,800	0
13	2024-T3 Bare	0.080	26,000	0
14	2024-T3 Bare	0.080	30,200	0
15	2024-T3 Bare	0.080	30,200	0
16	2024-T3 Bare	0.080	30,200	0
17	2024-T3 Bare	0.080	30,200	0
18	2024-T3 Clad	0.080	10,400	0
19	2024-T3 Bare	0.100	26,000	0
20	2024-T3 Bare	0.100	26,000	0
21	2024-T3 Bare	0.100	26,000	0
22	2024-T3 Bare	0.100	30,700	0
23	2024-T3 Bare	0.100	35,400	0
24	2024-T3 Bare	0.100	35,400	0
25	2024-T3 Clad	0.100	13,000	0
26	2024-T3 Clad	0.100	35,000	0
27	2024-T3 Clad	0.100	38,500	0
28	2024-T3 Bare	0.125	16,100	0
29	2024-T3 Bare	0.125	18,400	0
30	2024-T3 Bare	0.125	18,400	0
31	2024-T3 Clad	0.125	31,200	0
32	2024-T3 Clad	0.125	37,400	0
33	2024-T3 Clad	0.125	44,700	0
34	2024-T3 Clad	0.160	19,750	0
35	2024-T3 Clad	0.160	19,750	0
36	2024-T3 Clad	0.160	19,750	0
37	2024-T3 Clad	0.160	19,750	0
38	2024-T3 Clad	0.160	23,100	0
39	2024-T3 Clad	0.160	29,600	0
40	7075-T6 Clad	0.050	21,800	0
41	7075-T6 Clad	0.050	21,800	0
42	7075-T6 Clad	0.050	29,800	0
43	7075-T6 Clad	0.100	28,000	0
44	7075-T6 Clad	0.100	28,000	0
45	7075-T6 Clad	0.100	28,000	0
46	7075-T6 Clad	0.100	34,400	0
47	7075-T6 Clad	0.100	34,400	0
48	7075-T6 Clad	0.100	44,200	0
49	7075-T6 Clad	0.100	44,200	0

APPENDIX A (cont.)

Plate Number	Material	Thickness (in.)	σ_a (PSI)	$\beta = (\sigma_m / \sigma_a)$
50	7075-T6 Clad	0.100	52,500	0
51	7075-T6 Bare	0.120	14,800	0
52	7075-T6 Bare	0.120	31,200	0
53	7075-T6 Bare	0.120	34,800	0
54	7075-T6 Bare	0.120	42,500	0

Plate #1

<u>2a</u>	<u>Nx10³</u>
0.687	325
0.704	340
0.713	365
0.755	395
0.814	419
0.878	430
0.900	445
0.974	460
1.007	475
1.069	490
1.083	505
1.154	520
1.226	535
1.244	550
1.298	565
1.570	580
1.641	585

Plate #2

<u>2a</u>	<u>Nx10³</u>
0.328	55
0.353	65
0.407	75
0.423	85
0.460	95
0.510	105
0.549	117
0.597	130
0.638	145
0.793	160
0.855	170
0.883	180
0.984	190
1.067	200
1.141	210
1.225	215
1.465	220
1.563	225
1.782	230

Plate #3

<u>2a</u>	<u>Nx10³</u>
0.361	50
0.401	60
0.486	70
0.502	80

Plate #3 cont.

<u>2a</u>	<u>Nx10³</u>
0.553	91
0.600	100
0.659	110
0.711	120
0.854	130
1.047	135
1.107	137
1.247	140
1.319	142
1.330	143
1.431	145
1.589	147
1.664	148

Plate #4

<u>2a</u>	<u>Nx10³</u>
0.271	25
0.288	35
0.302	45
0.368	60
0.413	70
0.451	80
0.485	90
0.541	100
0.594	110
0.710	120
0.937	130
1.053	133
1.096	135
1.120	140
1.476	145
1.569	146
1.768	149

Plate #5

<u>2a</u>	<u>Nx10³</u>
0.361	50
0.401	60
0.486	70
0.502	80
0.553	91
0.600	100
0.659	110
0.711	120
0.854	130
1.047	135

Plate #5 cont.

<u>2a</u>	<u>Nx10³</u>
1.107	137
1.247	140
1.319	142
1.330	143
1.431	145
1.589	147
1.664	148

Plate #6

<u>2a</u>	<u>Nx10³</u>
0.238	0
0.241	6
0.243	12
0.256	36
0.278	59
0.281	77
0.287	95
0.304	116
0.319	140
0.336	160
0.350	178
0.377	200
0.403	224
0.419	243
0.442	262
0.468	282
0.489	298
0.516	316
0.546	332
0.576	347
0.619	364
0.646	374
0.693	389
0.748	405
0.800	417
0.860	429
0.941	443
1.095	461
1.195	471
1.296	479
1.393	486
1.454	490
1.513	494
1.592	498

Plate #7

<u>2a</u>	<u>Nx10³</u>
0.255	0
0.260	6
0.268	12
0.313	36
0.348	59
0.382	77
0.384	95
0.402	118
0.420	140
0.439	160
0.452	178
0.478	200
0.511	224
0.542	243
0.579	262
0.619	282
0.649	298
0.695	316
0.748	332
0.807	347
0.899	364
0.952	374
1.060	389
1.195	405
1.328	417
1.497	429
1.552	433

Plate #8

<u>2a</u>	<u>Nx10³</u>
0.282	155
0.296	175
0.312	190
0.340	205
0.368	218
0.393	230
0.419	240
0.449	250
0.478	260
0.505	270
0.538	280
0.578	290
0.630	300
0.683	310
0.748	320
0.827	330
0.922	340
1.039	350

Plate #8 cont.

<u>2a</u>	<u>Nx10³</u>
1.182	360
1.329	369
1.460	374
1.704	384

Plate #9

<u>2a</u>	<u>Nx10³</u>
0.303	90
0.363	125
0.436	155
0.495	175
0.549	190
0.619	205
0.697	218
0.784	230
0.873	240
0.921	245
0.978	250
1.031	255
1.099	260
1.174	265
1.222	268
1.254	270
1.301	272
1.348	275
1.458	280
1.538	284
1.632	287
1.716	290

Plate #10

<u>2a</u>	<u>Nx10³</u>
0.242	200
0.358	514
0.419	600
0.566	650
0.600	780
0.694	790
0.819	810
0.886	835
0.951	860
1.048	880
1.134	895
1.232	915
1.421	927
1.532	941
1.823	955

Plate #11

<u>2a</u>	<u>Nx10³</u>
0.232	0
0.245	90
0.267	200
0.354	342
0.432	514
0.518	600
0.546	650
0.642	730
0.711	790
0.741	810
0.835	835
0.886	860
0.889	880
0.936	895
1.011	915
1.054	927
1.121	941
1.166	955
1.265	970
1.362	986
1.476	1000
1.566	1020

Plate #12

<u>2a</u>	<u>Nx10³</u>
0.299	5
0.326	10
0.356	15
0.424	25
0.518	35
0.648	45
0.841	55
1.155	65
1.867	76

Plate #13

<u>2a</u>	<u>Nx10³</u>
0.238	0
0.279	1
0.318	3
0.350	5
0.382	7
0.436	10
0.504	13
0.581	16
0.683	19
0.823	22

Plate #13 cont.

<u>2a</u>	<u>Nx10³</u>
1.032	25
1.432	28
1.746	29

Plate #14

<u>2a</u>	<u>Nx10³</u>
0.299	1
0.366	3
0.432	5
0.509	7
0.604	9
0.720	11
0.904	13
1.317	15
1.580	15.8
1.744	16.25

Plate #15

<u>2a</u>	<u>Nx10³</u>
0.231	0
0.261	1
0.287	2
0.346	4
0.385	6
0.441	8
0.535	11
0.689	15
0.794	17
0.927	19
1.096	21
1.223	22
1.302	22.5
1.527	23.5

Plate #16

<u>2a</u>	<u>Nx10³</u>
0.281	1.0
0.310	2.5
0.364	5.0
0.423	7.5
0.516	11.0
0.598	13.0
0.787	16.0
1.153	18.5
1.295	19.0

Plate #16 cont.

<u>2a</u>	<u>Nx10³</u>
1.473	19.5
1.670	20.0

Plate #17

<u>2a</u>	<u>Nx10³</u>
0.280	1
0.319	2.25
0.341	3
0.366	4
0.434	6
0.528	8
0.658	10
1.048	13
1.428	14
1.674	14.3

Plate #18

<u>2a</u>	<u>Nx10³</u>
0.271	700
0.294	850
0.302	878
0.310	900
0.320	927
0.330	953
0.341	986
0.347	1,000
0.367	1,049
0.395	1,113
0.438	1,186
0.452	1,215
0.489	1,269
0.519	1,317
0.570	1,394
0.668	1,497
0.765	1,575
0.836	1,631
0.879	1,661
0.978	1,731
1.081	1,800
1.222	1,869
1.323	1,910
1.444	1,950
1.480	1,960
1.523	1,971
1.560	1,980

Plate #19

<u>2a</u>	<u>Nx10³</u>
0.289	2
0.346	5
0.363	6
0.382	7
0.401	8
0.422	9
0.439	10
0.488	12
0.532	14
0.593	15
0.654	18
0.719	20
0.792	22
0.889	24
0.982	26
1.033	27
1.096	28
1.161	29
1.235	30
1.316	31
1.408	32
1.516	33
1.647	34
1.798	35

Plate #20

<u>2a</u>	<u>Nx10³</u>
0.850	2.0
0.928	3.0
1.011	4.0
1.056	4.5
1.105	5.0
1.158	5.5
1.208	6.0
1.264	6.5
1.321	7.0
1.378	7.5
1.442	8.0
1.503	8.5
1.564	9.0
1.621	9.5
1.682	10.0
1.737	10.5

Plate #21

<u>2a</u>	<u>Nx10³</u>
0.256	0.5
0.266	1.0
0.278	1.5
0.290	2.0
0.310	3.0
0.328	4
0.345	5
0.361	6
0.378	7
0.396	8
0.419	9
0.436	10
0.464	11
0.483	12
0.508	13
0.532	14
0.560	15
0.587	16
0.618	17
0.652	18
0.688	19
0.735	20
0.767	21
0.806	22
0.852	23
0.900	24
0.950	25
0.999	26
1.059	27
1.121	28
1.196	29
1.272	30
1.370	31
1.478	32
1.593	33
1.766	34

Plate #22

<u>2a</u>	<u>Nx10³</u>
0.258	1
0.297	2
0.334	3
0.368	4
0.411	5
0.522	6
0.508	7
0.559	8
0.623	9
0.685	10

Plate #22 cont.

<u>2a</u>	<u>Nx10³</u>
0.763	11
0.850	12
0.944	13
1.051	14
1.171	15
1.300	16
1.443	17
1.609	18
1.758	19

Plate #23

<u>2a</u>	<u>Nx10³</u>
0.249	0.50
0.282	1
0.344	2
0.403	3
0.727	6
0.991	7
1.254	7.6

Plate #24

<u>2a</u>	<u>Nx10³</u>
0.322	0.50
0.370	1.00
0.410	1.50
0.457	2.00
0.508	2.50
0.562	3.00
0.637	3.50
0.702	4.00
0.796	4.50
0.853	4.75
0.913	5.00
0.984	5.25
1.082	5.50
1.254	5.80
1.451	6.00

Plate #25

<u>2a</u>	<u>Nx10³</u>
0.283	253
0.297	277
0.303	300
0.346	400
0.398	500

Plate #25 cont.

<u>2a</u>	<u>Nx10³</u>
0.454	600
0.530	703
0.569	750
0.621	800
0.744	905
0.897	995
1.046	1,052
1.117	1,071
1.228	1,100
1.336	1,120
1.410	1,135
1.477	1,146

Plate #26

<u>2a</u>	<u>Nx10³</u>
0.400	2
0.583	4
1.035	6
1.706	6.5

Plate #27

<u>2a</u>	<u>Nx10³</u>
0.318	1.0
0.401	2.0
0.459	3.0
0.624	4.5
0.802	5.5
0.978	6.2
1.067	6.4
1.193	6.6
1.343	6.8
1.633	7.0

Plate #28

<u>2a</u>	<u>Nx10³</u>
0.298	82
0.323	98
0.338	107
0.361	122
0.406	145
0.434	164
0.457	169
0.491	188
0.512	197
0.551	214

Plate #28 cont.

<u>2a</u>	<u>Nx10³</u>
0.587	226
0.626	240
0.700	261
0.767	275
0.811	285
0.863	294
0.932	306
1.004	316
1.073	324
1.127	331
1.248	334
1.338	352
1.431	361
1.538	370
1.606	375
1.675	380

Plate #29

<u>2a</u>	<u>Nx10³</u>
0.246	6
0.269	15
0.289	20
0.305	29
0.331	35
0.346	40
0.386	50
0.414	61
0.492	75
0.569	84
0.710	96
0.810	102
0.873	105
1.075	113
1.144	115
1.303	120
1.370	121
1.459	123
1.520	125

Plate #30

<u>2a</u>	<u>Nx10³</u>
0.258	35
0.304	47
0.334	56
0.359	64
0.411	78

Plate #30 cont.

<u>2a</u>	<u>Nx10³</u>
0.445	88
0.500	100
0.600	115
0.649	121
0.749	131
0.811	136
0.883	141
0.988	147
1.156	154
1.272	159
1.365	162
1.462	165
1.533	167
1.610	169

Plate #31

<u>2a</u>	<u>Nx10³</u>
0.291	1
0.338	2
0.376	3
0.419	4
0.461	5
0.508	6
0.560	7
0.653	8
0.698	9
0.783	10
0.897	11
1.025	12
1.269	13.2
1.360	13.5
1.482	13.8
1.587	14.0
1.734	14.2

Plate #32

<u>2a</u>	<u>Nx10³</u>
0.341	0.5
0.444	1.2
0.490	1.5
0.587	2.0
0.727	2.5
0.999	3.0
1.302	3.2
1.583	3.3
1.843	3.35

Plate #33

<u>2a</u>	<u>Nx10³</u>
0.297	0.1
0.347	0.2
0.422	0.4
0.495	0.6
0.581	0.8
0.729	1.0
0.856	1.1
1.073	1.2
2.029	1.3

Plate #34

<u>2a</u>	<u>Nx10³</u>
0.345	56
0.385	58
0.394	60
0.405	66
0.436	74
0.460	80
0.530	88
0.580	94
0.644	98
0.688	104
0.744	108
0.791	114
0.857	122
0.920	125
0.990	130
1.031	135
1.087	136
1.133	137
1.190	146
1.256	150
1.288	152
1.314	154
1.421	155
1.461	157
1.479	158
1.517	160

Plate #35

<u>2a</u>	<u>Nx10³</u>
0.257	7
0.260	20
0.280	30
0.341	40
0.394	48

Plate #35 cont.

<u>2a</u>	<u>Nx10³</u>
0.468	55
0.494	60
0.561	68
0.616	76
0.691	84
0.745	88
0.784	92
0.834	96
0.893	100
0.945	104
0.995	108
1.033	112
1.092	116
1.130	120
1.172	124

Plate #36

<u>2a</u>	<u>Nx10³</u>
0.384	51
0.422	56
0.453	60
0.475	65
0.515	70
0.560	75
0.583	80
0.630	86
0.688	92
0.799	100
0.840	104
0.893	108
0.915	112
0.965	116
1.056	120
1.185	124
1.239	126
1.314	128
1.426	132
1.547	135
1.601	137

Plate #37

<u>2a</u>	<u>Nx10³</u>
0.241	35
0.317	50
0.379	60
0.416	70

Plate #37 cont.

<u>2a</u>	<u>Nx10³</u>
0.477	80
0.512	90
0.602	100
0.648	105
0.703	110
0.768	116
0.819	123
0.951	131
1.046	138
1.104	141
1.227	146
1.329	152
1.388	156
1.520	161

Plate #38

<u>2a</u>	<u>Nx10³</u>
0.299	6
0.356	10
0.435	16
0.487	22
0.552	28
0.626	34
0.729	40
0.796	44
0.893	49
1.015	54
1.118	58
1.245	62
1.369	66
1.595	71

Plate #39

<u>2a</u>	<u>Nx10³</u>
0.367	6.0
0.486	9.0
0.605	13.0
0.700	15.5
0.792	17.5
0.930	20.0
1.067	22.5
1.167	24.0
1.246	25.0
1.335	26.0
1.438	27.2
1.530	28.5

Plate #40

<u>2a</u>	<u>Nx10³</u>
0.266	13
0.302	20
0.328	27
0.397	34
0.452	41
0.528	48
0.633	54
0.717	60
0.789	65
0.883	70
1.115	76
1.172	78
1.266	80
1.416	83
1.625	86

Plate #41

<u>2a</u>	<u>Nx10³</u>
0.219	0
0.338	35
0.360	40
0.415	45
0.443	50
0.470	55
0.577	65
0.642	70
0.685	75
0.756	80
0.835	85
0.939	90
1.053	95
1.245	100
1.499	103
1.653	105

Plate #42

<u>2a</u>	<u>Nx10³</u>
0.234	3
0.255	6
0.294	9
0.352	12
0.425	15
0.494	18
0.585	21
0.668	24
0.936	27

Plate #42 cont.

<u>2a</u>	<u>Nx10³</u>
1.178	30
1.530	32
1.774	33

Plate #43

<u>2a</u>	<u>Nx10³</u>
0.390	10
0.441	11
0.482	12
0.521	13
0.558	14
0.636	15
0.687	16
0.769	17
0.829	18
0.889	19
0.954	20
1.009	21
1.099	22
1.231	23
1.353	24
1.550	25
1.895	26

Plate #44

<u>2a</u>	<u>Nx10³</u>
0.250	5.0
0.247	5.5
0.252	6.0
0.266	6.5
0.268	7.0
0.274	7.5
0.338	12.0
0.390	13.0
0.448	13.5
0.434	14.0
0.455	14.5
0.460	15.0
0.475	15.5
0.500	16.0
0.524	16.5
0.553	17.0
0.578	17.5
0.584	18.0
0.613	18.5
0.628	19.0

Plate #44 cont.

<u>2a</u>	<u>Nx10³</u>
0.663	20.0
0.716	21.0
0.876	22.0
0.913	22.5
0.971	23.0
1.005	23.5
1.082	24.0
1.152	24.5
1.214	25.0
1.288	25.5
1.391	26.0
1.508	26.5
1.631	27.0
1.818	27.5
2.062	28.0

Plate #45

<u>2a</u>	<u>Nx10³</u>
0.247	30.0
0.234	30.5
0.307	31.0
0.322	31.5
0.327	33.0
0.354	33.5
0.362	34.0
0.364	34.5
0.388	35.0
0.395	35.5
0.405	36.0
0.410	36.5
0.422	37.0
0.434	38.0
0.470	39.0
0.480	39.5
0.493	40.0
0.514	40.5
0.527	41.0
0.540	41.5
0.549	42.0
0.572	42.5
0.600	43.5
0.620	44.0
0.660	45.0
0.690	46.0
0.725	46.5
0.751	47.0
0.772	47.5
0.814	48.0

Plate #45 cont.

<u>2a</u>	<u>Nx10³</u>
0.834	48.5
0.846	49.0
0.883	49.5
0.906	50.0
0.969	50.5
1.007	51.0
1.097	52.0
1.178	52.5
1.221	53.0
1.292	53.5
1.379	54.0
1.498	54.5
1.730	55.0
2.025	55.5

Plate #46

<u>2a</u>	<u>Nx10³</u>
0.195	0.0
0.216	0.5
0.233	1.0
0.262	1.5
0.277	2.0
0.305	2.5
0.327	3.0
0.351	3.5
0.368	4.0
0.395	4.5
0.428	5.0
0.451	5.5
0.466	6.0
0.490	6.5
0.525	7.0
0.552	7.5
0.591	8.0
0.613	8.5
0.645	9.0
0.688	9.5
0.732	10.0
0.759	10.5
0.819	11.0
0.895	11.5
0.932	12.0
1.002	12.5
1.052	13.0
1.133	13.5
1.196	14.0
1.278	14.5
1.406	15.0
1.611	15.5

Plate #46 cont.

<u>2a</u>	<u>Nx10³</u>
2.067	16.0

Plate #47

<u>2a</u>	<u>Nx10³</u>
0.222	0.0
0.300	2.5
0.321	3.0
0.339	3.5
0.362	4.0
0.376	4.5
0.403	5.0
0.434	5.5
0.458	6.0
0.486	6.5
0.511	7.0
0.550	7.5
0.565	8.0
0.644	9.0
0.701	9.5
0.748	10.0
0.802	10.5
0.864	11.0
0.944	11.6
1.013	12.0
1.127	12.5
1.303	13.0
1.805	13.6

Plate #48

<u>2a</u>	<u>Nx10³</u>
0.261	0.50
0.306	1.0
0.329	1.3
0.345	1.5
0.380	1.8
0.408	2.0
0.439	2.2
0.472	2.4
0.518	2.6
0.561	2.8
0.633	3.0
0.758	3.2
0.958	3.4
1.742	3.5

Plate #49

<u>2a</u>	<u>Nx10³</u>
0.242	0.2
0.273	0.5
0.305	0.8
0.325	1.0
0.382	1.5
0.427	2.0
0.453	2.2
0.523	2.6
0.635	3.0
0.666	3.1
0.723	3.2
0.769	3.3
0.845	3.4
0.930	3.5
1.037	3.55

Plate #50

<u>2a</u>	<u>Nx10³</u>
0.281	0.2
0.298	0.3
0.337	0.4
0.351	0.5
0.385	0.6
0.411	0.7
0.464	0.8
0.534	0.9
0.635	1.0
0.918	1.1
2.230	1.15

Plate #51

<u>2a</u>	<u>Nx10³</u>
0.273	800
0.335	830
0.391	855
0.443	875
0.527	905
0.656	930
0.799	950
1.030	970
1.202	980
1.308	985
1.429	990
1.567	995

Plate #52

<u>2a</u>	<u>Nx10³</u>
0.261	1
0.291	2
0.320	3
0.355	4
0.383	5
0.416	6
0.450	7
0.495	8
0.530	9
0.576	10
0.622	11
0.679	12
0.734	13
0.808	14
0.882	15
0.967	16
1.061	17
1.176	18
1.240	18.5
1.312	19
1.390	19.5
1.468	20
1.583	20.5
1.707	21

Plate #53

<u>2a</u>	<u>Nx10³</u>
0.243	1
0.275	2
0.309	3
0.343	4
0.387	5
0.423	6
0.486	7
0.540	8
0.599	9
0.670	10
0.756	11
0.851	12
0.962	13
1.028	13.5
1.101	14
1.180	14.5
1.266	15
1.366	15.5
1.476	16
1.551	16.3
1.617	16.5
1.728	16.8

Plate #54

<u>2a</u>	<u>Nx10³</u>
0.274	0.5
0.319	1.0
0.362	1.5
0.408	2.0
0.459	2.5
0.515	3.0
0.596	3.5
0.679	4.0
0.794	4.5
0.963	5.0
1.058	5.2
1.203	5.4
1.286	5.5
1.687	5.7

APPENDIX B

Crack Growth Data For Combined Loading,

2024-T3 Bare Aluminum

Plate Number	Thickness (in.)	Tensile Load PSI	Transverse Load LB.
1a	0.050	10,000	60
2a	0.050	10,000	80
3a	0.050	"	80
4a	0.050	"	100
5a	0.050	"	100
6a	0.050	"	125
7a	0.050	"	125
8a	0.050	"	150
9a	0.050	"	150
10a	0.050	"	175
11a	0.050	"	175
12a	0.050	"	200
13a	0.050	"	200

Plate #1a

<u>2a</u>	<u>Nx10³</u>
0.306	0.0
0.331	12.7
0.361	30.2
0.404	50.0
0.455	70.1
0.491	81.5
0.573	100.0
0.615	112.2
0.672	130.6
0.749	145.7
0.798	160.0
0.883	179.8
0.933	200.0

Plate #2a

<u>2a</u>	<u>Nx10³</u>
0.324	0
0.348	10.0
0.393	20.0
0.432	28.9
0.491	37.2
0.546	44.1
0.613	51.4
0.677	57.0
0.744	62.3
0.826	67.6
0.897	72.4
0.954	75.4
1.031	79.5
1.084	82.3
1.161	85.9
1.221	88.3
1.287	91.6
1.369	94.3
1.434	96.8
1.524	100.0
1.595	102.9
1.717	106.9
1.794	110.0
1.856	113.3

Plate #3a

<u>2a</u>	<u>Nx10³</u>
0.316	0.0
0.333	10.0
0.368	17.0
0.405	24.0

Plate #3a cont.

<u>2a</u>	<u>Nx10³</u>
0.452	30.0
0.511	36.8
0.560	43.6
0.616	49.0
0.688	54.3
0.754	60.0
0.826	64.9
0.883	68.7
0.953	72.4
1.012	76.5
1.121	81.4
1.158	85.8
1.235	90.2
1.280	94.0
1.366	99.0
1.447	103.0
1.537	106.9
1.612	110.0
1.704	114.5
1.814	119.0

Plate #4a

<u>2a</u>	<u>Nx10³</u>
0.376	0.0
0.452	7.6
0.535	13.4
0.615	18.6
0.702	24.6
0.829	30.1
0.907	33.6
0.984	37.5
1.071	41.0
1.167	45.2
1.247	49.5
1.336	52.6
1.419	58.6
1.497	61.8
1.615	67.1
1.685	71.1
1.785	74.0

Plate #5a

<u>2a</u>	<u>Nx10³</u>
0.319	0.0
0.360	8.2
0.422	14.5
0.474	20.1

Plate #5a cont.

<u>2a</u>	<u>Nx10³</u>
0.545	26.5
0.619	31.1
0.714	36.0
0.773	39.2
0.846	43.8
0.934	49.1
1.001	52.5
1.077	55.4
1.161	58.6
1.216	60.7
1.299	64.6
1.385	68.5
1.479	71.8
1.555	73.8
1.612	75.5
1.722	79.0
1.835	82.0
1.922	84.8

Plate #6a

<u>2a</u>	<u>Nx10³</u>
0.306	0.0
0.334	2.6
0.347	5.1
0.403	9.8
0.443	13.3
0.491	16.7
0.537	19.3
0.597	22.7
0.635	25.2
0.691	27.5
0.743	29.4
0.821	32.8
0.884	35.7
0.950	38.0
1.013	40.3
1.089	43.0
1.126	44.8
1.223	47.8
1.309	50.5
1.384	52.6
1.459	55.0
1.558	57.3
1.661	59.3
1.739	61.8

Plate #7a

<u>2a</u>	<u>Nx10³</u>
0.306	0.0
0.332	2.3
0.358	5.0
0.400	8.4
0.429	11.5
0.496	15.1
0.548	18.5
0.604	21.4
0.664	24.6
0.748	28.7
0.812	31.4
0.891	34.4
0.969	36.8
1.036	39.2
1.085	41.6
1.148	44.4
1.232	47.4
1.324	51.3
1.391	56.3

Plate #8a

<u>2a</u>	<u>Nx10³</u>
0.298	0.0
0.320	1.9
0.359	3.9
0.388	6.4
0.439	9.4
0.508	12.3
0.566	15.2
0.625	17.8
0.693	20.8
0.751	23.7
0.815	25.9
0.899	29.2
0.971	32.3
1.027	36.2
1.080	40.0

Plate #9a

<u>2a</u>	<u>Nx10³</u>
0.288	0.0
0.311	1.8
0.332	3.4
0.370	5.9
0.404	8.8
0.453	10.9
0.507	13.2

Plate #9a cont.

<u>2a</u>	<u>Nx10³</u>
0.567	16.4
0.598	18.5
0.682	21.3
0.725	22.6
0.774	24.3
0.844	27.1
0.915	29.6
0.969	31.9
1.041	34.5
1.120	36.5
1.176	38.4
1.248	42.7

Plate #10a

<u>2a</u>	<u>Nx10³</u>
0.294	0.0
0.312	1.3
0.360	3.7
0.406	6.3
0.458	8.6
0.525	10.9
0.585	13.2
0.629	14.6
0.665	17.6
0.784	19.8
0.842	22.7
0.979	29.3

Plate #11a

<u>2a</u>	<u>Nx10³</u>
0.283	0.0
0.304	1.6
0.325	3.1
0.364	5.8
0.406	8.5
0.450	10.2
0.489	12.1
0.538	15.3
0.574	17.4
0.641	20.9
0.737	23.4
0.797	27.4
0.889	30.3
0.942	33.3
1.011	34.7
1.069	35.9
1.160	38.8
1.233	40.6

Plate #11a cont.

<u>2a</u>	<u>Nx10³</u>
1.332	41.6
1.461	43.5

Plate #12a

<u>2a</u>	<u>Nx10³</u>
0.310	0.0
0.334	2.5
0.385	4.9
0.437	8.2
0.504	10.9
0.576	13.9
0.627	17.2
0.724	21.2
0.890	24.1
0.987	26.2
1.057	28.8
1.233	30.2
1.592	31.0

Plate #13a

<u>2a</u>	<u>Nx10³</u>
0.304	0.0
0.330	2.3
0.380	4.1
0.428	6.3
0.474	8.2
0.550	11.7
0.600	14.7
0.688	17.5
0.751	20.0
0.803	22.9
0.862	26.1
0.940	29.2
1.008	32.7
1.070	37.8

Appendix C

Material Properties

2024-T3

Thickness (in.)	Yield Strength (at 0.2% - KSI)	Tensile Strength (KSI)	% Elongation (2" gage length)
0.050 Clad	39.7	61.7	12.5
0.050 Bare	56.4	75.5	17.4
0.080 Bare	49.9	77.3	18.7
0.100 Bare	61.8	80.3	18.2
0.100 Clad		Not Available	
0.125 Bare	51.4	78.2	19.5
0.125 Clad		Not Available	
0.160 Clad	48.6	69.2	11.6

7075-T6

Thickness (in.)	Yield Strength (at 0.02% - KSI)	Tensile Strength (KSI)	% Elongation (2" gage length)
0.050 Clad	63.1	77.5	7.8
0.100 Clad	65.6	71.3	2.2
0.120 Bare	75.4	84.2	9.5